ACCSCIENCE PUBLISHING

International Journal of Bioprinting

ACCEPTED PAPER · MAIN TEXT

Effect of graphene and graphene oxide addition in crosslinking and mechanical properties of photocurable resins for stereolithography

Article ID: IJB4075

Citation: Armentia SLD, Giménez R, Real JCD, Serrano B, Cabanelas JC, Paz E. Effect of graphene and graphene oxide addition in crosslinking and mechanical properties of photocurable resins for stereolithography. *Int J Bioprint*. 2024. doi: 10.36922/ijb.4075

AccScience Publishing
RESEARCH ARTICLE
Volume X Issue X (2024)
doi: 10.36922/ijb.4075

Effect of graphene and graphene oxide addition in crosslinking and mechanical properties of photocurable resins for stereolithography

Running title: Effect of G/GO on photocurable resin structure

S. Lopez de Armentia [1*], R. Giménez [2], J.C. del Real [1], B. Serrano [2], J.C. Cabanelas [2], and E. Paz [1]

[1]Institute for Research in Technology/Mechanical Engineering Dept., Universidad Pontificia Comillas, Alberto Aguilera 25, 28015 Madrid, Spain

[2]Department of Materials Science and Engineering and Chemical Engineering, IAAB, University Carlos III of Madrid, 28911 Leganés, Spain

***Corresponding author:**
Sara Lopez de Armentia (sara.lopez@comillas.edu)

Citation: Armentia SLD, Giménez R, Real JCD, Serrano B, Cabanelas JC, Paz E. Effect of graphene and graphene oxide addition in crosslinking and mechanical properties of photocurable resins for stereolithography. *Int J Bioprint*. 2024. doi: 10.36922/ijb.4075

Received: June 28, 2024
Revised: August 13, 2024
Accepted: August 14, 2024
Published Online: August 15, 2024

Abstract

The mechanical properties of the resins used in stereolithography are often inadequate, prompting studies on their enhancement with nanofillers such as graphene-based nanomaterials (GBNs). GBNs hold promise for enhancing the mechanical performance of photocurable resins, yet their incorporation often leads to unexpected alterations that impact the final nanocomposite. The full spectrum of GBN effects on these resins remains incompletely understood, with many studies reporting suboptimal improvements. This study aims to elucidate the influence of graphene (G) and graphene oxide (GO) on the mechanical properties and polymer structure of an acrylic photocurable resin used in stereolithography. The novelty of this research lies in examining how GBNs affect the polymer structure during polymerization and the degree of crosslinking—parameters that have not been sufficiently explored—and correlating these effects with photopolymerization outcomes. Stereolithography is particularly valuable in biomedicine thanks to its exceptional precision in creating patient-specific models, functional parts, implant devices or scaffolds for tissue engineering, but also various other innovative uses across different industries.

Through comprehensive tensile tests, DMTA, DSC, FTIR, and microscopy analyses, it was found that GO enhances tensile strength but reduces the crosslinking degree, thus hindering overall improvements. These findings highlight the critical roles of nanomaterial dispersion, matrix-polymer interaction, and reinforcement in affecting proper crosslinking. Future studies should investigate the impact of varying nanoparticle sizes on crosslinking to further validate these hypotheses.

Keywords: Graphene-Based Nanomaterials; Photocurable Resin; Stereolithography; DMTA; Crosslinking

1. Introduction

Additive manufacturing (AM) technologies have revolutionized the field of materials science by enabling the fabrication of complex geometries with high precision and reduced waste. Among various AM techniques, Vat Polymerization technologies, based on the use of photocurable resins such as stereolithography (SLA), have gained significant attention due to their ability to produce high-resolution parts with excellent surface finish [1].

One of the most promising examples of the use of photocurable resins is in the biomedical field, where their application has gained significant popularity in recent years [2,3]. This growth is driven by the development and commercialization of resins certified for biomedical applications. As a result, there has been a proliferation of applications, including the creation of patient-specific models and functional parts, implantable devices, particularly in dentistry, and short-term implantable devices. The ability to produce highly accurate and customized medical components has made Vat Polymerization techniques indispensable in modern medical practice. While the biomedical field represents a key area of application, photocurable resins are also being explored for various other innovative uses across different industries [4].

The incorporation of graphene-based nanomaterials (GBN), such as graphene (G) and graphene oxide (GO), into UV-curable resins has opened up new avenues for enhancing the mechanical and functional properties of materials fabricated through Vat Polymerization technologies [5]. The unique two-dimensional structure of G, characterized by a single layer of carbon atoms arranged in a hexagonal lattice, imparts exceptional mechanical strength, electrical conductivity, and thermal stability [6]. GO, a derivative of G, offers additional functional groups that can facilitate dispersibility and bonding within the polymer matrix.

One of the most promising aspects of GBN-reinforced resins is the potential improvement in mechanical properties. Studies have shown that even a minor incorporation of G or GO can yield substantial increases in tensile strength, Young's modulus, and fracture toughness [7–9]. Beyond mechanical enhancements, GBNs have also demonstrated the capacity to improve thermal and electrical conductivity in photocurable resins. Consequently, this advancement has pushed the development of UV-curable resins with multifunctional properties, suitable for applications that range from structural designs to electronics and thermal management [5,10].

It has been demonstrated that achieving proper dispersion of GBN within the polymeric matrix is crucial for unlocking the full potential of these nanomaterials in enhancing composite properties [11]. Various techniques, including ultrasonication, functionalization of GBNs, and the use of surfactants, have been employed to ensure the uniform distribution of these nanomaterials within UV-curable resins [7,12,13]. It is interesting to highlight that the chemical functionalization of GO is easier than G thanks to its oxygen-containing functional groups [14].

Nevertheless, integrating G and GO into photocurable resins for 3D printing poses unique challenges, like the low content of printable G and GO, high cost, and uncured photosensitive resins. Contrary to expectations, several studies have found that the addition of these nanomaterials does not consistently enhance the mechanical properties of these resins, even with adequate dispersion [13,15,16]. The most significant challenges include insufficient curing of the resin due to nanoparticle absorption of UV light, the induction of anisotropy in composites caused by the inherent alignment of G sheets, increased internal stresses from resin shrinkage, and compromised adhesion between layers. However, the precise nature and extent of these effects remain incompletely understood, necessitating further research to comprehensively discern their mechanisms and conditions, thereby facilitating the optimization of the development of these materials.

In the context of layer adhesion and internal stresses, it has been observed that the presence of GBN can either enhance or hinder these properties. This variation largely depends on their interaction with the polymer matrix, distribution, and dispersibility. On one hand, GBNs, due to their rigid structure, could potentially mitigate these stresses by providing a reinforcing network. Conversely, non-uniform dispersion or aggregation of GBNs can intensify internal stresses, counteracting their potential reinforcing benefits.

In relation to the challenge of achieving an adequate degree of polymerization, a significant issue arises with the use of GBN in photocurable 3D printing materials. G strongly absorbs light, especially at the critical photopolymerization wavelength of around 405 nm, impeding sufficient light penetration to the polymer resin [17]. This often results in under-polymerization of the polymer matrix, leading to a notable decrease in stiffness and strength when compared to the base polymer without G [17]. Several researchers have concentrated their efforts on enhancing the mechanical properties of SLA 3D printed samples by employing various post-treatment methods

aimed at ensuring complete resin curing. These investigations have demonstrated that post-treatment highly affects the properties of the final material [18,19]. Despite these efforts, it appears that these approaches do not fully resolve the issue, indicating that the problem of achieving optimal mechanical properties in SLA-G-printed materials extends beyond merely ensuring complete curing of the resins.

Finally, the anisotropy effect in the GBN-reinforced photocurable resins is an intriguing phenomenon that has been attributed to the Self-selection of Naturally Aligned Graphene (SNAG) effect [10,12,20,21] . SNAG is a proposed process caused by the light-blocking properties of G due to their strong absorbance of photopolymerizing light. This reduction in light transmission creates a shadowing effect, preventing sufficient laser light from reaching the photosensitive resin behind the G for polymerization and solidification. In the SNAG effect, horizontally oriented G platelets are particularly effective in blocking laser light and preventing polymerization. As a result of this selective alignment of G platelets, the composite material presents enhanced stiffness and strength of the polymer in the direction of the G alignment. However, while this SNAG effect can be advantageous in terms of improving material properties, it also poses challenges in achieving consistent and predictable 3D printing outcomes with G-reinforced photocurable resins.

In summary, while GBNs have the potential to significantly improve the mechanical properties of 3D-printed objects, their actual impact can be complicated by various factors inherent to the additive manufacturing process. Understanding and controlling these factors are essential for optimizing the reinforcing effect of GBNs in UV-curable resins used in Vat Polymerization technologies. Although several of these complex factors have already been studied, much work remains to be done to fully understand their global effects, particularly in cross-linking, which has not been thoroughly explored. Given these complexities, the aim of this paper is to explore the influence of adding G and GO on the polymeric structure and crosslinking. We hypothesize that these nanomaterials can significantly alter the polymeric structure by affecting the curing of the resin and, therefore, mechanical properties of photocurable resins can be affected. Previous research has not thoroughly examined this aspect, and our study seeks to fill this gap, contributing to the optimization of these advanced materials.

2. Materials and methods

2.1. Materials

Commercially available photocurable resin Clear V4 (Formlabs, Somerville, MA, USA) with the following composition: 55-75% urethane dimethacrylate, 15-25% methacrylate monomer(s) and <0.9% Diphenyl(2,4,6-trimethylbenzoyl)phosphine oxide (TPO) photoinitiator.

The Clear resin was reinforced with two different graphene-based nanomaterials (GBN): graphene (G) and graphene oxide (GO). G powder was composed of 1-2 layers of G sheets with an average lateral size of 2-4 μm supplied by Avanzare Nanotechnology (La Rioja, Spain) and GO powder had a thickness of 0.7-1.2 μm and average lateral size of 4-8 μm supplied by NanoInnova Technologies (Toledo, Spain). Micrographs taken with a scanning electron microscope (SEM) TENEO-LoVac (Eindhoven, the Netherlands) are shown in Figure 1. From those micrographs, the lateral size has been measured, being 7.1 ± 1.9 μm and 11.9 ± 2.7 μm for G and GO, respectively. The measured size is larger than the value given by the manufacturer due to the natural agglomeration of these nanofillers.

2.2. Experimental methodology

2.2.1. Sample preparation

Dispersion of nanomaterials inside the matrix is a crucial factor in achieving improvements in mechanical properties. Due to the high viscosity of Clear resin, methyl methacrylate (MMA) supplied by Sigma Aldrich (St. Louis, Missouri, USA) was used to disperse the nanomaterials powders by ultrasonication following the procedure explained in previous researchs [17]. In short, G and GO were sonicated with MMA and resin was gradually added with sonication steps. The ratio resin:MMA was 300:10 v/v. The frequency range applied was 1985–2050 kHz at a 50% amplitude for 10 ± 0.5 min—pulses of 10 ± 0.5 s ON and 20 ± 0.5 s OFF. This process was followed by degassing to avoid the presence of microbubbles that could affect mechanical properties. Samples of as-received Clear resin ® and resin reinforced with 0.05 %wt. of G (R+G) and GO (R+GO) were prepared.

The printed samples were obtained by stereolithography with SLA printer Form2 (Formlabs, Somerville, MA, USA). Layer thickness was set at 100 μm and the wavelength used was 405 nm.

Exposure time was set by the manufacturer specifications, but it was adapted in the case of R+G samples since these had shown printability issues [13], then it was increased an 8.9% to achieve enough polymerization degree to obtain parts. The other parameters were already set by the manufacturer. The samples were cleaned for 3 minutes with isopropyl alcohol (IPA) in FormWash (Formlabs) equipment. Post-curing was realized in FormCure chamber (Formlabs). During this process, samples were subjected to UV and heat. Parameters used were 405 nm of wavelength, 80°C and 90 minutes. Samples without post-curing (as-printed) and with post-curing treatment (post) were studied in order to determine the effect of the post-curing treatment in the resin properties.

2.2.2. Differential Scanning Calorimetry (DSC)

The DSC measurements were performed using a Mettler-Toledo Differential Scanning Calorimetry, DSC 882e (Greifensee, Switzerland). Dynamic scans from 20 to 250°C at 20°C/min were carried out and STARe software (Mettler Toledo) was used to analyze the curves. 5-10 mg samples were placed into aluminum crucibles with a capacity of 40 µL and 50 µm hole in the lid. Nitrogen was the purge gas and was delivered at a rate of 80 mL/min. Two scans were carried out. In the first scan, the area of the curing peak was measured to determine if the polymer was completely cured and it could be completely polymerized by the application of heat, whilst in the second scan, glass transition temperature (Tg) was determined as the midpoint of the step of the baseline through the endothermal direction. At least, 3 samples per condition were tested and averaged.

2.2.3. Fourier-Transformed Infrared Spectroscopy (FTIR)

Infrared spectra were obtained with an IRT-5200 FTIR spectrometer from Jasco (Jasco Analitica Spain, Madrid, Spain), with attenuated total reflectance (ATR) technique. DuraSample Diamond accessory formed by a 0.5 mm diameter diamond embedded in a ZnSe crystal was used. The ratio signal-to-noise is better than 8000:1 (5.4 · 10−5 noise absorbance). Spectra were recorded with a resolution of 4 cm−1 from 4000 to 400 cm −1 by taking 32 scans.

Double bond conversion (DBC) was studied following the peaks corresponding to carbonyl groups (C=O) at 1728 cm^{-1} and the peak corresponding to acrylate double bond (C=C) located at 810 cm^{-}

[1] [22]. As reference, liquid resin with or without GBN was used [23], using the following equation (I).

$$DBC = \left[1 - \frac{I_{(C=C)}}{I_{liquid(C=C)}} \cdot \frac{I_{liquid(C=O)}}{I_{(C=O)}}\right] \cdot 100 \qquad \text{(I)}$$

2.2.4. Tensile tests

To carry out tensile tests, dog bone samples were obtained following ISO 527-2:2012 standard (sample 1BA) [24]. Printed layers formed 85° with the applied load direction. Tests were conducted using a Universal Testing Machine IBTH/500 (Ibertest, Madrid, Spain) with a load cell of 5 kN, operating at a elongation rate of 3 mm/min. The tensile strength, Young Modulus and Elongation at break were calculated using the load versus elongation until failure data.

2.2.5. Dynamic Mechanical Thermal Analysis (DMTA)

Dynamic mechanical thermal characterization DMTA Q800 (TA instrument, Delaware, USA) of post-cured samples was performed with printed rectangular specimens (15.3 x 5.0 x 1.4 mm) in tension mode in a temperature range of 30-225 °C, at a single frequency of 1 Hz and a heating rate of 2 °C/min. As in tensile tests, layers were printed with an angle of 85° with the applied load.

With the data obtained from DMTA, it was possible to calculate the molecular weight between crosslinks in a thermosetting resin. Firstly, storage modulus had to be measured within the rubbery plateau region (E'rubbery) and, from that value and applying equation (II), molecular weight between crosslinks (M_c) could be calculated [25]:

$$M_c = \frac{3 \cdot R \cdot T \cdot \rho}{E'_{rubbery}} \qquad \text{(II)}$$

Where R is the universal gas constant, T is the absolute temperature at which the modulus was calculated (448 K) and ρ is the density of the polymer. Density was obtained applying Archimedes' Principle with a Density Kit (Mettler Toledo, Greifensee, Switzerland).

Besides, crosslinking density per unit volume was calculated following equation (III) [26]:

$$d = \frac{E'_{rubbery}}{3 \cdot R \cdot (T_g + 40)} \qquad \text{(III)}$$

Where T_g is the glass transition temperature (K).

2.2.6. Scanning Electronic Microscopy (SEM)

Field Emission Scanning Electron Microscopy (FESEM) was carried out in a TENEO-LoVac (Eindhoven, Nederland). Images were obtained from cryogenic fracturing and sputter-coating with gold.

2.2.7. Statistical analysis

The results were further analyzed for statistical significance using a one-way analysis of variance (ANOVA) test with a post hoc Scheffe's test (SPSS 28.0 for Windows; IBM SPSS, USA). A P-value of less than 0.05 was considered to indicate statistical significance.

3. Results

3.1. Differential Scanning Calorimetry (DSC)

DSC thermograms were analyzed to determine the presence of unpolymerized resin and the Tg of each sample. From the first scan, it is possible to ascertain whether polymerization be completed with the application of heat to the printed sample. Polymerization process appears as an exothermal peak in DSC thermogram, therefore the presence of any exothermal peak in this first scan may indicate that the polymerization has not been fully complete. The results of the first scan for each material, as-printed and after post-curing treatment (post) are shown in

Table ***1***. Values were calculated as the average ± standard deviation of the 3 performed experiments.

The results of the first scan showed a similar polymerization heat for all the as-printed samples (around 15 J/g), being the differences inside the precision of the measurements. However, GBN-loaded resins (R+G and R+GO) showed a significant higher peak temperature, which means that GBN showed a retardation effect in the polymerization reaction [27].

Post-cured samples did not exhibit a peak, suggesting that the post-curing process may have achieved complete polymerization in all cases. It is important to consider that DSC primarily determines thermal curing; the absence of a peak might indicate that further curing through heat application is no longer feasible. However, a clear distinction was observed between the post-cured and non-post-cured samples.

The Tg calculated form the second scan was also showed in

Table ***1***. It was found that during the printing process, R+G and R+GO showed lower Tg. When samples were post-cured, Tg increased in every case, this can be attributed to an increase in the crosslinking degree of samples because the application of UV-light together with heat [18].

3.2. Fourier-Transformed Infrared Spectroscopy (FTIR)

It is well-known that a problem that UV-photocurable acrylic resins present is that the percentage of carbon-carbon double bond that are converted into single bonds to obtain a polymer is low, which results in deficient mechanical properties [28]. DBC was calculated for every sample and results are shown in

Table ***2***.

Analyzing the DBC results of as-printed samples revealed that the addition of GBN (G and GO) produced a slight reduction of DBC during the printing process, compared to R. When the post-treatment was carried out, it was found a slight increase in DBC conversion, although this increase was less notable for G resin. In all cases, the degree of conversion was around 50% with similar values reported in other studies [29]. The residual unreacted double bonds could exist either as free unreacted monomer or as pendant groups within the polymer network.

3.3. Tensile tests results

Besides tensile strength, tensile tests gave also information about the stiffness of samples and its elasticity through Young's modulus and elongation at break. The three parameters obtained are shown in Table 3, and a representative curve for each sample is shown in Figure 2.

The tensile strength of as-printed samples was significantly lower when both GBN types were added, with this reduction been particularly notable in the case of G. The reduction was about 18% in the case of R+GO and 38% in R+G. This decrease in mechanical properties was accompained by a decrease in Young's modulus, wich also was more pronunced for R+G. Regarding the elongation at break, a sligh increase was observed only in the R+GO.

In all cases, post-curing enhanced the tensile strength and rigidity of the samples while reducing their elongation at break compared to the as-printed samples. This improvement may be attributable to increased polymerization and crosslinking, resulting in lower chains mobility.

After post-curing, R+GO samples exhibited significantly higher tensile strength than R (5% higher), whereas R+G samples continued to show lower strength. Interestingly, R+GO still showed a lower Young´s Modulus compared to R and R+G.

Considering that as-printed R+G and R+GO samples showed similar DBC values, the observed differences in mechanical properties do not seem proportional to the DBC reduction. This suggests that the differences are not solely due to low polymerization caused by GBN presence. This deduction is further supported by the post-cured mechanical results, where the lack of correlation between DBC and mechanical properties persists. While post-curing does enhance mechanical properties, this improvement may be originated not only from increased polymerization but also from enhanced crosslinking within the polymeric matrix.

Furthermore, the reduction in Young's modulus for both, as-printed and post-cured samples, aligns with the observed decrease in Tg upon GBN addition. This correlation suggests that variations in mechanical properties are related to the crosslinking and changes in molecular structure of each composite.

3.4. FESEM Microscopy analysis

The aspect and roughness of fracture surfaces provide insightful information about materials behavior, such as brittleness or ductility, and the crack deviation mechanism. This crack deviation typically manifests as shift in the crack growth plane because micro-cracks encounter stiff GBN and bypass them [30]. SEM micrographs in Figure 3 shows the differences in post-cured R, R+G and R+GO samples. In post-cured R and R+G samples, the surfaces were smooth, lacking any noticeable undulations, indicative of brittle fracture characteristics. This observation suggests that the addition of G does not significantly alter the crack path, likely due to inadequate adhesion or interaction with the resin matrix (see Figure 3b). In contrast, post-cured R+GO (Figure 3c) corresponds to a more ductile fracture pattern, showing homogeneously distributed undulations (shown with red arrows), which indicated a reasonably uniform dispersion of GO and a ductile fracture. Surface undulations often signal an increased fracture toughness, primarily because they absorb more fracture energy, thereby improving the matrix capacity to withstand damage [31,32]. This more ductile behavior observed in the fracture of R+GO samples should be reflected in the mechanical properties; while post-curing enhanced tensile strength in R+GO, the transition from the brittle fracture of R to the more ductile nature of R+GO is more pronounced than the observed

increase in tensile strength values. This significant observation will be further discussed in the results discussion section.

3.5. DMTA results

The DMTA tests were exclusively conducted on post-cured samples, as the as-printed specimens exhibited a sticky consistency that could damage the testing equipment. Furthermore, the focus on post-cured samples aligns with their relevance to the final application, with as-printed samples being studied just for comparative purposes to understand the impact of post-curing on the properties of resins. The storage modulus (Figure 4a), loss modulus (Figure 4b) and tan δ (Figure 4c) parameters were obtained from these tests for each material: R, R+G and R+GO.

The initial zone of the obtained curves, at lower temperatures, corresponds to the glassy state of the polymer/nanocomposite. In this zone, it was found that both, storage (E') and loss modulus (E'') exhibited high values. As the temperature rises, free polymeric segments started to move and the excess of energy was dissipated as heat. Subsequently, this results in a noticeable decrease in both E' and E'' values, marking glass transition phase. After glass transition, E', E'' and tan δ decreased because the material passes the rubbery state. Curves showed that only one transition occurred during the heating. It suggested that all the samples analyzed were completely polymerized and only a physical transition could be observed, which corresponded to the glass transition [18].

The temperature of the peak on tan δ (Tα) corresponds to the glass transition temperature. It was found that DSC and DMTA detected similar temperatures and the minor differences could be due to the heating rate used to do the DSC scans. However, they also presented a small shoulder (Tα') before the glass transition, which could be attributed to a sub-Tg [33]. This reflects that there are segments of the polymerized network that relax more quickly, at lower temperatures, and therefore exhibit greater mobility. To facilitate the analysis of the results, all the data explained in this paragraph are summarized in Table 4.

The results showed that the modulus of R and R+G are very similar, while GO produced a reduction in E' and tan δ peak. It suggested that GO interacted with the polymer chains, probably inhibiting the crosslinking. It could also be observed by the full width at half height (ΔTα), which is higher for R+GO sample, as can be seen in Figure 4c and Table 4. The higher ΔTα also suggested

that a less homogeneous network was formed [18]. The printing process and the post-treatment resulted in different networks, with different crosslinking degrees and linearity, which was demonstrated in the different Tgs found.

The interaction of the acrylic resin with GO should be better than with G, which is more apolar and lacks oxygenated functionalities. Therefore, if the interfacial interaction is greater, the stiffness of the interface should also be higher, which would not lower the Tα [34]. However, this is precisely what happened: with both reinforcements, the Tα of the bulk decreased. This could be explained by a lower degree of curing due to the presence of graphene[17]. Moreover, the rise in tan δ was more gradual, especially in R+GO (as seen by a broadening in the transition). A possible explanation is that there was an interfacial subregion with increased mobility due to the disruption of the polymerized network, which was more pronounced in GO because it has a larger interface area due to better dispersion. In densely crosslinked polymers, this interface may act as a free surface where the chains exhibit greater mobility and faster relaxation [35].

R and R+G showed similar temperatures for final tan δ maximum, as well as the rubbery modulus. It suggested that the same final structure was obtained [36]. However, the addition of GO changed these values, resulting in a different final structure. It was already found for the kinetics curves, where a different polymerization rate was shown by R+GO samples [17].

The polymer structure was analyzed by calculating molecular weight between crosslinks (M_c), the obtained results are presented in Table 5. It can be observed that the Mc for R+GO is higher compared to R and R+G, indicating a less crosslinked structure in the polymer after post-curing. Conversely, the M_c value for R+G was very similar to the R, suggesting that the presence of G did not significantly impact the crosslinking density in the final polymer structure. These conclusions are confirmed through the analysis of crosslinking density values.

3.6. Adhesion between layers

Due to the inherent nature of 3D-printed specimens, which are created layer by layer rather than as a purely continuous material, a decrease in the quality of layer adhesion or overall printing quality can negatively affect the final mechanical properties of the resulting material. For this reason, the samples were analyzed by optical microscopy to determine the layer adhesion and the surface quality. The detail of the interface between the layers is visible in Figure 5. The impact of

different GBN on the superficial aspect and the interface between layers could explain the variations found in mechanical properties. GO had the smallest effect on printing quality, with only some marks visible due to the presence of the nanofiller. In the case of G, the surface was not smooth, displaying many imperfections, which could potentially affect mechanical performance at the macroscale.

4. Discussion

The aim of this study is to explore the factors that can affect the success of GBN as reinforcement agents in photocurable acrylic resins. The peculiar polymerization process of these resins makes it difficult to determine the factors that may influence the final polymer structure and performance.

Previous research has already identified some of the factors that could affect the performance of nanocomposites, including the dispersion quality of the nanofiller [37,38], chemical interaction between the reinforcement and the matrix [39,40], and the impact of nanomaterials on the curing degree [17,41]. However, other effects have gone unnoticed, such as the effect of the nanofiller on the final three-dimensional structure of the polymer chains. This structure is known to directly influence the polymer properties; for example, changing crosslinking degree in thermosetting polymers directly correlates with mechanical strength [42,43]. While nanoparticles are known to enhance mechanical properties by different mechanisms, acting as crack stoppers and deflectors [44], if their presence leads to a decrease in other polymer properties such as curing degree or crosslinking, the expected improvements may not be observed. This is evidenced in this study by adding G and GO to a photocurable acrylic resin for use in stereolithography 3D printing.

To understand whether G and GO affect the curing degree, DSC and FTIR tests were conducted. Previous studies indicate that G and GO in these photocurable acrylic resins affect the polymerization [17,45] kinetics and mechanism, potentially impacting mechanical properties. The results show that the curing degree is not significantly affected by GO, especially after postcuring, although a slight decrease is detected in the case of G. This aligns with previous studies [46] demonstrating that G can hinder light from reaching the photoinitiator, thus affecting curing. However, this effect is less pronounced with the addition of GO.

Figure 6 presents a schematic representation of this effect. When UV light reaches the uncured resin, a portion of the light is absorbed by graphene (G), preventing it from reaching the

photoinitiator and thus inhibiting the initiation of the polymerization process. In contrast, graphene oxide (GO) does not absorb UV light; instead, it acts as a radical scavenger. GO combines with the activated photoinitiator, which prevents effective crosslinking and results in a less crosslinked polymer network. This demonstrates the differing impacts of G and GO on the polymerization process and the final polymer structure.

Even without nanofillers, it has been found that UV-polymerized acrylic resins typically exhibit low carbon-carbon double bond conversion. It is related with a low polymerization and crosslinking degree. Post-curing slightly improves this conversion but remains around 50% for all samples. However, DSC analysis indicates complete curing in post-cured samples, suggesting that residual double bonds are probably pendant in the polymer network.

While the polymerization degree appears unaffected, differences are observed in glass transition temperature (Tg) and mechanical properties, which decrease with the presence of GBNs. This suggests that nanofillers may adversely affects mechanical properties due to poor dispersion or interaction with the matrix, and/or alteration of the molecular structure of the resulting polymer [38,47].

Besides previous considerations, additive manufacturing present a new parameter to consider when studying the mechanical performance of parts obtained by this technology. The observed decrease or lack of expected improvement in mechanical properties could result from reduced interlayer adhesion due to the presence of GBN. Microscopic analysis does not reveal poor interlayer adhesion but indicates lower print quality with G, likely due to increased imperfections and defects, contributing to the negative effect on mechanical properties. In relation to the effect of printing parameters on the mechanical properties of printed parts, it is worth mentioning that other studies have also reported correlations between mechanical properties, printing process peculiarities, and crosslinking of the polymeric structure. For example, previous research has found that the frequency of UV curing and the resulting crosslinking density play crucial roles. These studies demonstrated that as layer thickness decreases from 200 μm to 50 μm, higher crosslinking density is induced, increasing Young's modulus due to more densely spaced crosslinked layers. However, when the layer thickness is reduced to 25 μm, an unexpected decrease in Young's modulus is observed [48]. This decrease is attributed to insufficient inter-layer crosslinking, as there are not enough monomers available between each crosslinked layer to ensure

efficient stress transfer, resulting in a lower modulus. In our study, the layer thickness has been kept constant in all samples, but this mechanism is similar to the effect observed with the addition of GO, when it acts as radical scavenger.

The SEM images (Figure 3) provide crucial insights into the dispersion of GBN and its correlation with the fracture behavior of the material. The R+GO sample, following the applied dispersion protocols, exhibits an optimal degree of dispersion. The GO is uniformly distributed and shows strong interaction with the polymer matrix, being well-integrated within it. This homogeneity results in an irregular fracture surface, indicating enhanced toughness. In contrast, the dispersion of G is markedly inferior, characterized by the presence of distinct clusters (Figure 3b). Consequently, the fracture surface is smooth, corroborating the poor interaction with the polymer matrix.

These findings align well with the observed mechanical properties. In the postcured R+G sample, there is an increase in Young's modulus and a decrease in elongation, attributed to the rigidity effect of the introduced G. However, this effect is less pronounced due to poor nanoparticle dispersion. In contrast, the GO sample exhibits a decrease in Young's modulus compared to G and an increase in elongation. This can be explained by reduced crosslinking, which leads to significant disruption of the polymer network, resulting in greater deformability and a lower modulus. In the R+GO sample, the reinforcing effect of GO is present but is offset and surpassed by the antagonistic effect of reduced crosslinking. The impact of GO on the crosslinking of the polymer network could be mitigated through surface modifications such as silanization, as previously demonstrated by Uysal et al. [49]. In their study, it was shown that silanization of the surface of nanomaterials can significantly enhance the physical and chemical properties of the polymer network.

It's noteworthy that R+GO fracture surface exhibit significantly more ductility, showing uniformly dispersed undulations. This suggests that GO nanoparticles may effectively provide obstacles to the crack propagation [8,50]. This observation indicates that the lack of expected improvements may be the result of a change in the polymer structure, particularly from a crosslinking perspective.

The polymer crosslinking degree is evident in the calculated molecular weight between crosslinks (Mc) after post-curing. Results indicate that R+GO exhibits a less crosslinked polymer structure. This could be attributed to the larger size of GO, which impedes proper formation of the reticulated

network structure, resulting in a less crosslinked matrix and consequently weaker mechanical performance. Conversely, while G appears to have no significant impact on the crosslinking of the final polymer matrix, possibly due to its smaller size and lower chemical reactivity compared to GO, the observed poor mechanical properties may result from inadequate dispersion, incomplete curing, or poor G integration into the matrix. This conclusion is supported by the observation of the fracture surface, where a ductile behaviour is not found.

5. Conclusion

The study aimed to investigate factors influencing the effectiveness of graphene-based nanomaterials (GBNs) in photocurable acrylic resins for stereolithography. While previous research identified several factors affecting nanocomposite performance, including nanofiller dispersion and chemical interactions, this study revealed that GBN may also produce effects on polymer chain structure.

The presence of graphene (G) and graphene oxide (GO) nanoparticles in acrylic resins for 3D printing did not significantly affect polymerization degree, but impacted mechanical properties and glass transition temperature. Differences in mechanical properties between samples indicate that GBNs may have different effects in the resin. Particularly, GO produced a slight increase in tensile strength (5%), but it was found that it led to a less crosslinked matrix, potentially due to its larger size. In the case of G, it showed poor mechanical properties possibly due to inadequate dispersion or integration, without affecting crosslinking degree.

Therefore, the observed differences between the various nanocomposites are due to changes induced in the resin structure by the presence of the nanofillers, rather than the effect of the nanofillers themselves.

Funding

This work was supported by Comillas Pontifical University (grant number PP2020_08).

Conflict of interest

The authors declare they have no competing interests.

Author contributions

Conceptualization: S. Lopez de Armentia, E. Paz
Investigation: S. Lopez de Armentia, R. Gimenez, B. Serrano, E. Paz
Methodology: J.C. del Real, J.C. Cabanelas
Formal analysis: S. Lopez de Armentia, R. Gimenez, J.C. del Real, B. Serrano, J.C. Cabanelas, E. Paz
Writing – original draft: S. Lopez de Armentia, E. Paz
Writing – review & editing: R. Gimenez, J.C. del Real, B. Serrano, J.C. Cabanelas

Ethics approval and consent to participate

Not applicable.

Consent for publication

Not applicable.

Availability of data

Contact corresponding author.

References

[1] R.V. Pazhamannil, P. Govindan, Current state and future scope of additive manufacturing technologies via vat photopolymerization, Materials Today: Proceedings 43 (2021) 130–136. https://doi.org/10.1016/j.matpr.2020.11.225.

[2] F. Alifui-Segbaya, Biomedical photopolymers in 3D printing, RPJ 26 (2019) 437–444. https://doi.org/10.1108/RPJ-10-2018-0268.

[3] F.P.W. Melchels, J. Feijen, D.W. Grijpma, A review on stereolithography and its applications in biomedical engineering, Biomaterials 31 (2010) 6121–6130. https://doi.org/10.1016/j.biomaterials.2010.04.050.

[4] A. Al Rashid, W. Ahmed, M.Y. Khalid, M. Koç, Vat photopolymerization of polymers and polymer composites: Processes and applications, Additive Manufacturing 47 (2021) 102279. https://doi.org/10.1016/j.addma.2021.102279.

[5] C.M. Shebeeb, M.B. Afif, L. Jacob, D. Choi, H. Butt, Vat photopolymerisation 3D printing of graphene-based materials, Virtual and Physical Prototyping 18 (2023) e2276250. https://doi.org/10.1080/17452759.2023.2276250.

[6] A. Al Rashid, S.A. Khan, S. G. Al-Ghamdi, M. Koç, Additive manufacturing of polymer nanocomposites: Needs and challenges in materials, processes, and applications, Journal of Materials Research and Technology 14 (2021) 910–941. https://doi.org/10.1016/j.jmrt.2021.07.016.

[7] M. Alsaadi, E.P. Hinchy, C.T. McCarthy, V.F. Moritz, A. Portela, D.M. Devine, 3D Printing of Photocurable Resin Reinforced by Functionalised Graphene Nanoplatelets, Materials Proceedings 14 (2023) 20. https://doi.org/10.3390/IOCN2023-14540.

[8] E. Paz, F. Forriol, J.C. del Real, N. Dunne, Graphene oxide versus graphene for optimisation of PMMA bone cement for orthopaedic applications, Materials Science and Engineering: C 77 (2017) 1003–1011. https://doi.org/10.1016/j.msec.2017.03.269.

[9] S. He, N.D. Petkovich, K. Liu, Y. Qian, C.W. Macosko, A. Stein, Unsaturated polyester resin toughening with very low loadings of GO derivatives, Polymer 110 (2017) 149–157. https://doi.org/10.1016/j.polymer.2016.12.057.

[10] G. Zhang, D. Song, J. Jiang, W. Li, H. Huang, Z. Yu, Z. Peng, X. Zhu, F. Wang, H. Lan, Electrically assisted continuous vat photopolymerization 3D printing for fabricating high-performance ordered graphene/polymer composites, Composites Part B: Engineering 250 (2023) 110449. https://doi.org/10.1016/j.compositesb.2022.110449.

[11] A. Liang, X. Jiang, X. Hong, Y. Jiang, Z. Shao, D. Zhu, Recent Developments Concerning the Dispersion Methods and Mechanisms of Graphene, Coatings 8 (2018) 33. https://doi.org/10.3390/coatings8010033.

[12] K. Markandan, C.Q. Lai, Enhanced mechanical properties of 3D printed graphene-polymer composite lattices at very low graphene concentrations, Composites Part A: Applied Science and Manufacturing 129 (2020) 105726. https://doi.org/10.1016/j.compositesa.2019.105726.

[13] S.L. de Armentia, S. Fernández-Villamarín, Y. Ballesteros, J.C. Del Real, N. Dunne, E. Paz, 3D Printing of a Graphene-Modified Photopolymer Using Stereolithography for Biomedical Applications: A Study of the Polymerization Reaction, Int J Bioprint 8 (2022) 503. https://doi.org/10.18063/ijb.v8i1.503.

[14] B.D. Holt, Z.M. Wright, A.M. Arnold, S.A. Sydlik, Graphene oxide as a scaffold for bone regeneration, WIREs Nanomedicine and Nanobiotechnology 9 (2017) e1437. https://doi.org/10.1002/wnan.1437.
[15] Universidade Católica Portuguesa, Faculdade de Medicina Dentária, Viseu, Portugal, H. Salgado, J. Fialho, Escola Superior de Tecnologia e Gestão, Instituto Politécnico de Viseu, Viseu, Portugal, M. Marques, INEGI – Instituto de Ciência e Inovação em Engenharia Mecânica e Engenharia Industrial, Porto, Portugal, M. Vaz, Universidade do Porto, Faculdade de Engenharia, Porto, Portugal, M. Figueiral, Universidade do Porto, Faculdade de Medicina Dentária, Porto, Portugal, P. Mesquita, Universidade do Porto, Faculdade de Medicina Dentária, Porto, Portugal, Mechanical and surface properties of a 3D-printed dental resin reinforced with graphene, J.Rpemd 64 (2023) 12–19. https://doi.org/10.24873/j.rpemd.2023.03.1050.
[16] M.M. Hanon, A. Ghaly, L. Zsidai, Z. Szakál, I. Szabó, L. Kátai, Investigations of the Mechanical Properties of DLP 3D Printed Graphene/Resin Composites, ACTA POLYTECH HUNG 18 (2021) 143–161. https://doi.org/10.12700/APH.18.8.2021.8.8.
[17] S. Lopez De Armentia, J. Abenojar, Y. Ballesteros, J.C. Del Real, N. Dunne, E. Paz, Polymerization Kinetics of Acrylic Photopolymer Loaded with Graphene-Based Nanomaterials for Additive Manufacturing, Nanomaterials 12 (2022) 4498. https://doi.org/10.3390/nano12244498.
[18] C. Mendes-Felipe, D. Patrocinio, J.M. Laza, L. Ruiz-Rubio, J.L. Vilas-Vilela, Evaluation of postcuring process on the thermal and mechanical properties of the Clear02^{TM} resin used in stereolithography, Polymer Testing 72 (2018) 115–121. https://doi.org/10.1016/j.polymertesting.2018.10.018.
[19] I.K. Cingesar, M.-P. Marković, D. Vrsaljko, Effect of post-processing conditions on polyacrylate materials used in stereolithography, Additive Manufacturing 55 (2022) 102813. https://doi.org/10.1016/j.addma.2022.102813.
[20] K. Markandan, I.P. Seetoh, C.Q. Lai, Mechanical anisotropy of graphene nanocomposites induced by graphene alignment during stereolithography 3D printing, Journal of Materials Research 36 (2021) 4262–4274. https://doi.org/10.1557/s43578-021-00400-5.
[21] C.Q. Lai, K. Markandan, B. Luo, Y.C. Lam, W.C. Chung, A. Chidambaram, Viscoelastic and high strain rate response of anisotropic graphene-polymer nanocomposites fabricated with stereolithographic 3D printing, Additive Manufacturing 37 (2021) 101721. https://doi.org/10.1016/j.addma.2020.101721.
[22] V. Jančovičová, M. Mikula, B. Havlínová, Z. Jakubíková, Influence of UV-curing conditions on polymerization kinetics and gloss of urethane acrylate coatings, Progress in Organic Coatings 76 (2013) 432–438. https://doi.org/10.1016/j.porgcoat.2012.10.010.
[23] G. Arias-Ferreiro, A. Ares-Pernas, A. Lasagabáster-Latorre, N. Aranburu, G. Guerrica-Echevarria, M.S. Dopico-García, M.-J. Abad, Printability Study of a Conductive Polyaniline/Acrylic Formulation for 3D Printing, Polymers 13 (2021) 2068. https://doi.org/10.3390/polym13132068.
[24] ISO 527-2:2012 Plastics - Determination of tensile properties - Part2: Test conditions for moulding and extrusion plastics, n.d.
[25] Quantifying Polymer Crosslinking Density Using Rheology and DMA - TA Instruments, (n.d.). https://www.tainstruments.com/applications-notes/quantifying-polymer-crosslinking-density-using-rheology-and-dma/ (accessed March 26, 2024).

[26] J. Zheng, Z.M. Png, S.H. Ng, G.X. Tham, E. Ye, S.S. Goh, X.J. Loh, Z. Li, Vitrimers: Current research trends and their emerging applications, Materials Today 51 (2021) 586–625. https://doi.org/10.1016/j.mattod.2021.07.003.
[27] S.H. Ryu, J.H. Sin, A.M. Shanmugharaj, Study on the effect of hexamethylene diamine functionalized graphene oxide on the curing kinetics of epoxy nanocomposites, European Polymer Journal 52 (2014) 88–97. https://doi.org/10.1016/j.eurpolymj.2013.12.014.
[28] M.L. Berlanga Duarte, L.A. Reyna Medina, P. Torres Reyes, S.C. Esparza González, A.M. Herrera González, Dental restorative composites containing methacrylic spiroorthocarbonate monomers as antishrinking matrixes, J of Applied Polymer Sci 136 (2019) 47114. https://doi.org/10.1002/app.47114.
[29] F. Alifui-Segbaya, J. Bowman, A.R. White, R. George, I. Fidan, Characterization of the Double Bond Conversion of Acrylic Resins for 3D Printing of Dental Prostheses, Compend Contin Educ Dent 40 (2019) e7–e11.
[30] B. Ahmadi-Moghadam, M. Sharafimasooleh, S. Shadlou, F. Taheri, Effect of functionalization of graphene nanoplatelets on the mechanical response of graphene/epoxy composites, Materials & Design (1980-2015) 66 (2015) 142–149. https://doi.org/10.1016/j.matdes.2014.10.047.
[31] D.A. Hawkins, A. Haque, Fracture Toughness of Carbon-Graphene/Epoxy Hybrid Nanocomposites, Procedia Engineering 90 (2014) 176–181. https://doi.org/10.1016/j.proeng.2014.11.833.
[32] W. Guo, Y. Yang, C. Liu, W. Bu, F. Guo, J. Li, E. Wang, Z. Peng, H. Mai, H. You, Y. Long, 3D printed TPMS structural PLA/GO scaffold: Process parameter optimization, porous structure, mechanical and biological properties, Journal of the Mechanical Behavior of Biomedical Materials 142 (2023) 105848. https://doi.org/10.1016/j.jmbbm.2023.105848.
[33] A. Sharma, X. Pan, J.M. Bjuggren, D. Gedefaw, X. Xu, R. Kroon, E. Wang, J.A. Campbell, D.A. Lewis, M.R. Andersson, Probing the Relationship between Molecular Structures, Thermal Transitions, and Morphology in Polymer Semiconductors Using a Woven Glass-Mesh-Based DMTA Technique, Chem. Mater. 31 (2019) 6740–6749. https://doi.org/10.1021/acs.chemmater.9b01213.
[34] A. Jiménez-Suárez, R. Moriche, S.G. Prolongo, M. Sánchez, A. Ureña, GNPs Reinforced Epoxy Nanocomposites Used as Thermal Interface Materials, JNanoR 38 (2016) 18–25. https://doi.org/10.4028/www.scientific.net/JNanoR.38.18.
[35] K.W. Putz, M.J. Palmeri, R.B. Cohn, R. Andrews, L.C. Brinson, Effect of Cross-Link Density on Interphase Creation in Polymer Nanocomposites, Macromolecules 41 (2008) 6752–6756. https://doi.org/10.1021/ma800830p.
[36] J.L. Vilas, J.M. Laza, M.T. Garay, M. Rodríguez, L.M. León, Unsaturated polyester resins cure: Kinetic, rheologic, and mechanical dynamical analysis. II. The glass transition in the mechanical dynamical spectrum of polyester networks, Journal of Polymer Science Part B: Polymer Physics 39 (2001) 146–152. https://doi.org/10.1002/1099-0488(20010101)39:1<146::AID-POLB130>3.0.CO;2-A.
[37] L.B.T. La, H. Nguyen, L.C. Tran, X. Su, Q. Meng, H.-C. Kuan, J. Ma, Exfoliation and dispersion of graphene nanoplatelets for epoxy nanocomposites, Advanced Nanocomposites 1 (2024) 39–51. https://doi.org/10.1016/j.adna.2023.10.001.
[38] L.-C. Tang, Y.-J. Wan, D. Yan, Y.-B. Pei, L. Zhao, Y.-B. Li, L.-B. Wu, J.-X. Jiang, G.-Q. Lai, The effect of graphene dispersion on the mechanical properties of graphene/epoxy composites, Carbon 60 (2013) 16–27. https://doi.org/10.1016/j.carbon.2013.03.050.

[39] E. Paz, Y. Ballesteros, J. Abenojar, N. Dunne, J.C. del Real, Advanced G-MPS-PMMA Bone Cements: Influence of Graphene Silanisation on Fatigue Performance, Thermal Properties and Biocompatibility, Nanomaterials 11 (2021) 139. https://doi.org/10.3390/nano11010139.
[40] K. Hu, D.D. Kulkarni, I. Choi, V.V. Tsukruk, Graphene-polymer nanocomposites for structural and functional applications, Progress in Polymer Science 39 (2014) 1934–1972. https://doi.org/10.1016/j.progpolymsci.2014.03.001.
[41] A. Surnova, D. Balkaev, D. Musin, R. Amirov, A.M. Dimiev, Fully exfoliated graphene oxide accelerates epoxy resin curing, and results in dramatic improvement of the polymer mechanical properties, Composites Part B: Engineering 162 (2019) 685–691. https://doi.org/10.1016/j.compositesb.2019.01.020.
[42] L.E. Nielsen, Cross-Linking–Effect on Physical Properties of Polymers, Journal of Macromolecular Science, Part C 3 (1969) 69–103. https://doi.org/10.1080/15583726908545897.
[43] A. Shokuhfar, B. Arab, The effect of cross linking density on the mechanical properties and structure of the epoxy polymers: molecular dynamics simulation, J Mol Model 19 (2013) 3719–3731. https://doi.org/10.1007/s00894-013-1906-9.
[44] C. Gao, T. Liu, C. Shuai, S. Peng, Enhancement mechanisms of graphene in nano-58S bioactive glass scaffold: mechanical and biological performance, Scientific Reports 4 (2014). https://doi.org/10.1038/srep04712.
[45] M. Sharif, B. Pourabbas, M. Sangermano, F. Sadeghi Moghadam, M. Mohammadi, I. Roppolo, A. Fazli, The effect of graphene oxide on UV curing kinetics and properties of SU8 nanocomposites, Polymer International 66 (2017) 405–417. https://doi.org/10.1002/pi.5271.
[46] R. Moriche, J. Artigas, L. Reigosa, M. Sánchez, S.G. Prolongo, A. Ureña, Modifications induced in photocuring of Bis- GMA/TEGDMA by the addition of graphene nanoplatelets for 3D printable electrically conductive nanocomposites, Composites Science and Technology 184 (2019) 107876. https://doi.org/10.1016/j.compscitech.2019.107876.
[47] Y.-J. Wan, L.-C. Tang, D. Yan, L. Zhao, Y.-B. Li, L.-B. Wu, J.-X. Jiang, G.-Q. Lai, Improved dispersion and interface in the graphene/epoxy composites via a facile surfactant-assisted process, Composites Science and Technology 82 (2013) 60–68. https://doi.org/10.1016/j.compscitech.2013.04.009.
[48] P.S. Borella, L.A.S. Alvares, M.T.H. Ribeiro, G.F. Moura, C.J. Soares, K. Zancopé, G. Mendonça, F.P. Rodrigues, F.D. Das Neves, Physical and mechanical properties of four 3D-printed resins at two different thick layers: An in vitro comparative study, Dental Materials 39 (2023) 686–692. https://doi.org/10.1016/j.dental.2023.06.002.
[49] E. Uysal, M. Çakir, B. Ekici, Graphene oxide/epoxy acrylate nanocomposite production via SLA and importance of graphene oxide surface modification for mechanical properties, Rapid Prototyping Journal 27 (2021) 682–691. https://doi.org/10.1108/RPJ-06-2020-0114.
[50] N.D. Alexopoulos, Z. Paragkamian, P. Poulin, S.K. Kourkoulis, Fracture related mechanical properties of low and high graphene reinforcement of epoxy nanocomposites, Composites Science and Technology 150 (2017) 194–204. https://doi.org/10.1016/j.compscitech.2017.07.030.

Figures and Tables

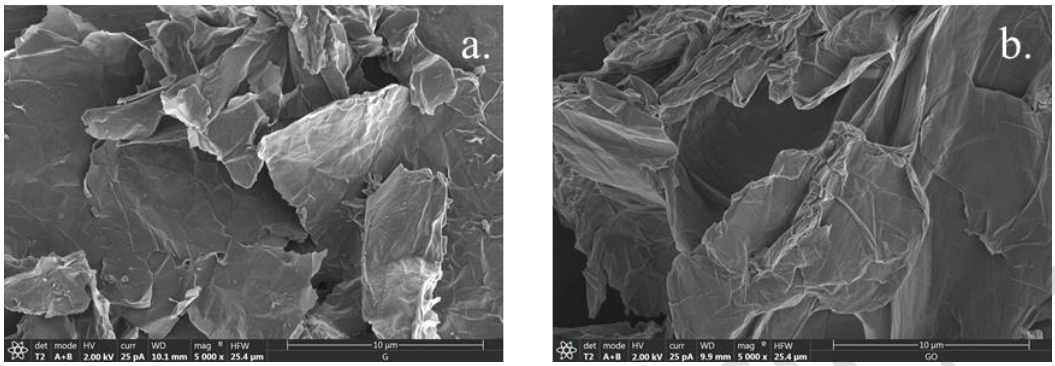

Figure 1. SEM images of G (a) and GO (b).

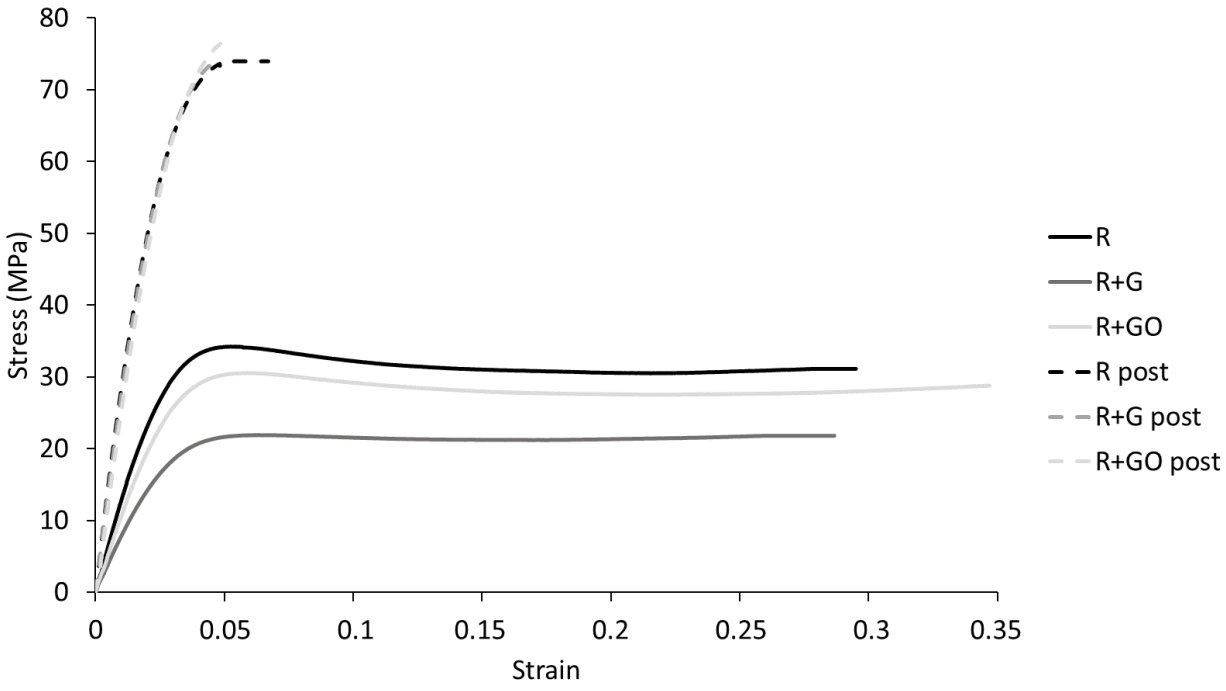

Figure 2. Stress-strain curves obtained from tensile tests.

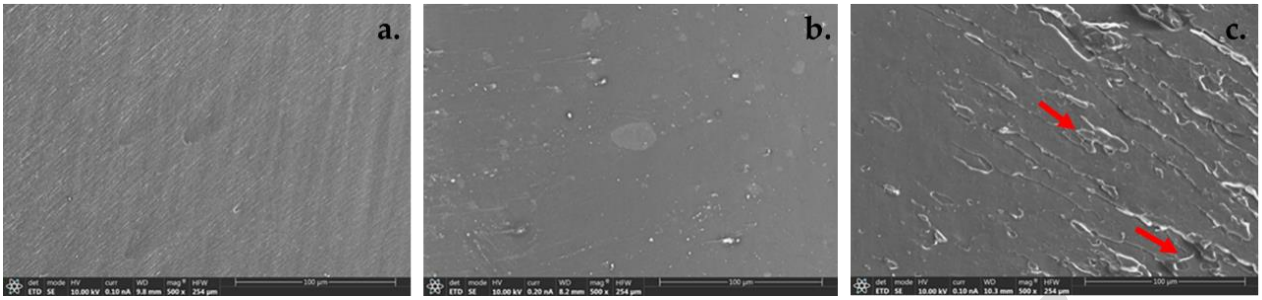

Figure 3. SEM micrographs of the fracture surface of post-cured R (a), R+G (b) and R+GO (c).

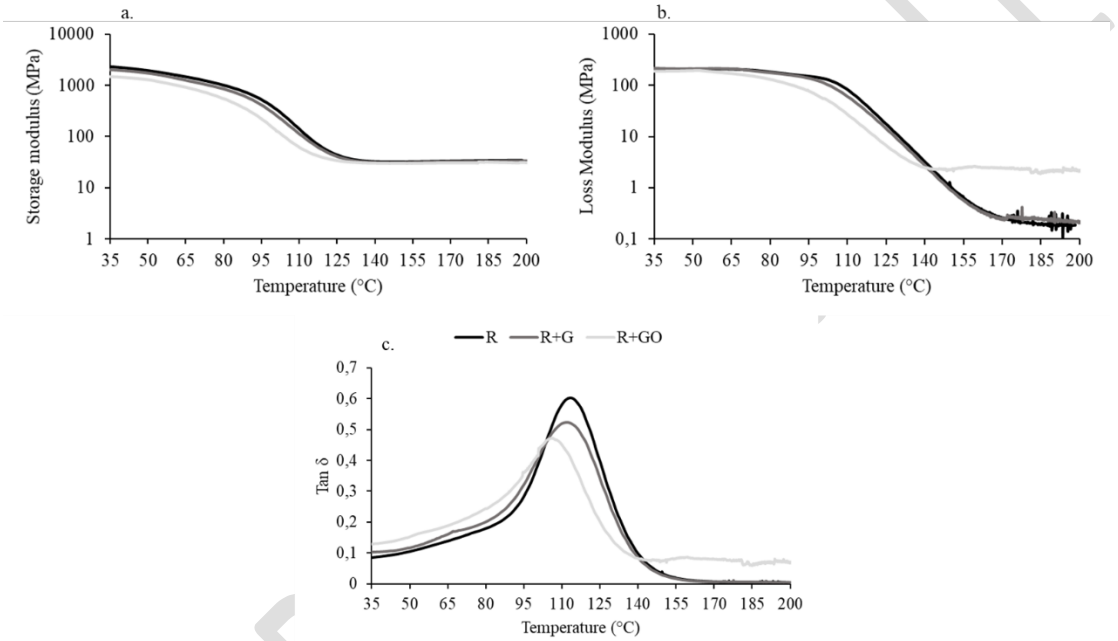

Figure 4. (a) Storage modulus (E'), (b) loss modulus (E''), and (c) tan δ of postcured R, R+G and R+GO samples.

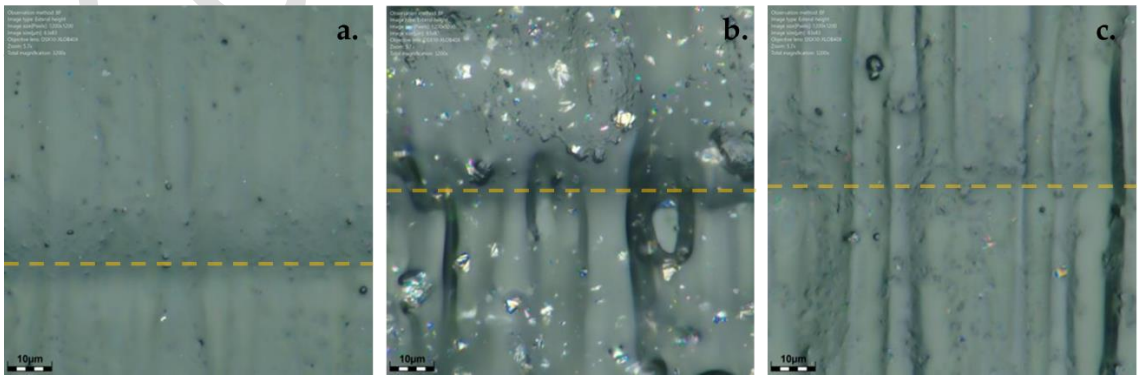

Figure 5. Surface analysis of printed samples of post-cured R, R+G and R+GO samples. The interface between printed layers was marked with the yellow line.

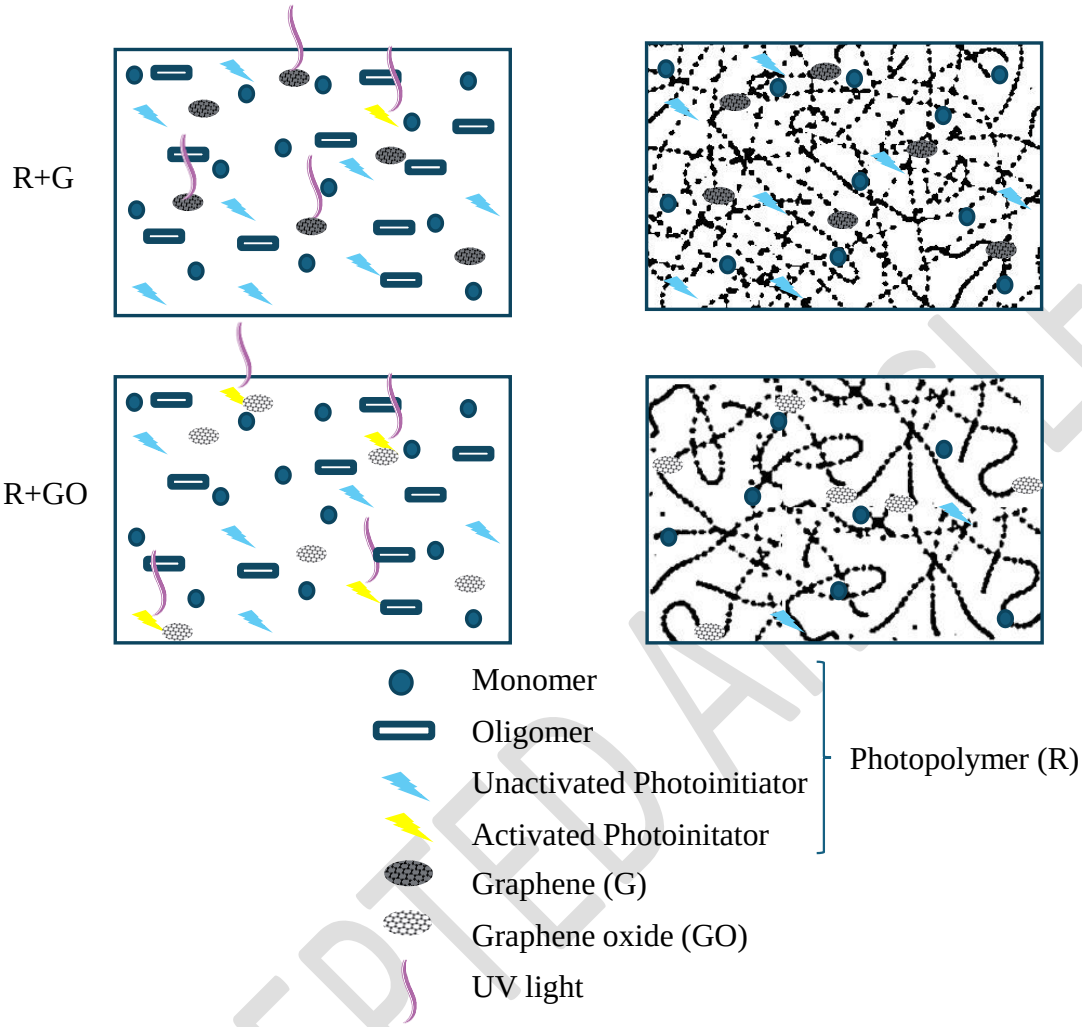

Figure 6. Schematic representation of the effects of G and GO on the photopolymerization process of the resin.

Table 1. Average Area and temperature (T) ± SD of polymerization peak (- means that no polymerization peak is observed), and T_g (°C) of as-printed and post-cured samples of R, R+G and R+GO.

	Polymerization peak				***Glass Transition Temperature***	
	as-printed		***post***		***as-printed***	***post***
	Area (J/g)	T (°C)	Area (J/g)	T (°C)	Tg (˚C)	Tg (˚C)
R	16 ± 4	165 ± 3	-	-	109 ± 3	117 ± 3
R+G	14 ± 3	175 ± 3	-	-	104 ± 6	110 ± 4
R+GO	13 ± 5	173 ± 4	-	-	103 ± 4	110 ± 2

Table 2. Double bond conversion (DBC) of samples with the studied post-treatment.

	As-printed	*Post*
R	48.6	51.6
R+G	46.0	48.6
R+GO	46.3	50.4

Table 3. Average tensile strength, Young's modulus and elongation at break ± SD of R, R+G and R+GO samples with the studied post-treatments. * means significantly different than R ($p < 0.05$)

		R	***R+G***	***R+GO***
As-printed	***Tensile Strength (MPa)***	34.49 ± 0.52	21.27 ± 1.52*	28.41 ± 3.87*
	Young's modulus (GPa)	1.29 ± 0.06	0.87 ± 0.34*	1.06 ± 0.13*
	Elongation at break (%)	29.49 ± 8.56	28.66 ± 4.39	34.80 ± 3.87
Post-cured	***Tensile Strength (MPa)***	73.79 ± 1.28	70.06 ± 4.23	77.55 ± 1.06*
	Young's modulus (GPa)	2.50 ± 0.13	2.72 ± 0.28	1.88 ± 0.39*
	Elongation at break (%)	6.68 ± 1.52	4.80 ± 1.11*	5.25 ± 0.49

Table 4. Summary of DMTA results.

	E' glass (GPa)	***E' rubbery (MPa)***	***E'' glass (GPa)***	***T_α (°C)***	***$T_{\alpha'}$ (°C)***	***ΔT_α (°C)***
R post	2.26	31.5	0.19	115	75	33.9
R+G post	2	32.7	0.2	112	68	38.0
R+GO post	1.47	28.6	0.19	106	53	52.9

Table 5. Density (ρ), molecular weight between crosslinks (M_c) and crosslinking density (d) of post-cured samples.

	ρ (g/cm^3)	M_c (g/mol)	d (mol/m^3)
R post	1.185	400.0	$2.95 \cdot 10^{-3}$
R+G post	1.181	401.4	$3.08 \cdot 10^{-3}$
R+GO post	1.182	437.3	$2.74 \cdot 10^{-3}$